

Utility Function-Based Real-Time Control of A Battery-Ultracapacitor Hybrid Energy System

He Yin, *Student Member, IEEE*, Chen Zhao, *Student Member, IEEE*, Mian Li, Chengbin Ma, *Member, IEEE*

Abstract—This paper discusses a utility function-based control of a battery-ultracapacitor hybrid energy system. The example system employs the battery semi-active topology. In order to represent different performance and requirements of the battery and ultracapacitor packs, the two packs are modeled as two independent but related agents using the NetLogo environment. Utility functions are designed to describe the respective preferences of battery and ultracapacitor packs. Then the control problem is converted to a multi-objective optimization problem solved by using the Karush-Kuhn-Tucker conditions. The weights in the objective functions are chosen based on the location of the knee point in the Pareto set. Both the simulation and experimental results show the utility function-based control provides a comparable performance with the ideal average load demand-based control, while the exact pre-knowledge of the future load demand is not required. The utility function-based control is fast enough to be directly implemented in real time. The discussion in this paper gives a starting point and initial results for dealing with more complex hybrid energy systems.

Index Terms—Battery, ultracapacitor, hybrid energy system, energy management, optimization control.

I. INTRODUCTION

Currently, batteries are one of the most commonly used energy storage devices. However, their energy and power densities, reliability, cycle-life and management are always their limitations, and thus batteries alone often cannot meet load requirements efficiently and continuously. A hybrid energy system, formed by combining multiple energy storage devices (e.g., battery, ultracapacitor, flywheel, fuel cell, etc.) and generators (e.g., micro-turbine, wind turbine, PV panel, etc.), has proved to be a feasible solution to meet the energy/power requirements with improved flexibility, reliability and cost efficiency. Since the system configuration and behavior of the hybrid system are becoming more complex, the optimized management and control of a hybrid energy system is still a challenging task. To achieve the optimal solution to this energy management problem, it is especially important to represent and take advantage of the characteristics of each

component and the interactive relationship among them. Compared to centralized control approaches, modeling and control of the components as independent but related agents fully respect the performance and requirements of various individual components [1]. This agent-based approach can improve the synergy, and thus, the flexibility, scalability, fault-tolerance and reliability of the hybrid energy systems, and also can reduce required computational efforts [2]–[4].

This paper discusses the modeling and control of a battery semi-active hybrid energy storage system (HESS). Although the structure of this type of HESSs is relatively simple, those typical systems have been widely applied and are suitable for agent-based modeling and control. The discussion in this work provides a starting point and initial results for dealing with more complex hybrid energy systems. The battery-ultracapacitor HESSs have been investigated in recent years. The basic concept is to use ultracapacitors (UCs) as an assistant energy storage device in order to improve the performance of the entire energy storage systems, in terms of efficiency, reliability, and dynamic response. UCs provide fast and efficient energy delivery and long cycle-life without any chemical reaction involved [5], [6]. In addition, the state of charge (SOC) of an UC can be accurately obtained because its SOC is proportional to the square of the cell voltage. The range of UC operating temperature (-40 to +70°C) is also wider than that of batteries. The primary disadvantage of UCs is their relatively low energy density compared to batteries. Thus hybridization of batteries (and/or fuel cells) and UCs is considered in nature to be the best usage of UCs for real applications [7]–[9].

Besides the hardware aspects, many energy management strategies have been proposed for the control of the battery-ultracapacitor HESSs [10], [11]. A real-time optimal-control approach was discussed and implemented using Neural Networks (NNs) [12]. This approach was further improved by introducing a pre-training procedure to obtain convergent weights for NNs [13]. The rule-based approaches were shown to be suitable for the control of the battery-ultracapacitor HESS [14]–[18]. Model predictive control is able to handle various constraints in the HESSs [19], and a probability-weighted Markov process has been used to predict future load demands [20]. The trade-off between the battery protection and the minimization of energy loss has been addressed by using a multi-objective optimization approach [21]. Meanwhile, in terms of extending battery cycle-life and improving the system efficiency, it is ideal to let batteries satisfy the average load demand (ALD) (i.e., a constant current), and thus UCs provide all the dynamic load current [22]–[24]. Without considering

Manuscript received March 14, 2014; revised May 30, 2014, and October 7, 2014; accepted November 13, 2014. This work was supported by National Science Foundation of China [grant number 51375299(2014-2017) and 51375302(2014-2017)].

Copyright (c) 2009 IEEE. Personal use of this material is permitted. However, permission to use this material for any other purposes must be obtained from the IEEE by sending a request to pubs-permissions@ieee.org

The authors are all with University of Michigan-Shanghai Jiao Tong University Joint Institute, Shanghai Jiao Tong University, 800 Dongchuan Road, Minhang, Shanghai 200240, P. R. China (e-mail: yyy@sjtu.edu.cn; zc437041363@sjtu.edu.cn; mianli@sjtu.edu.cn; chbma@sjtu.edu.cn). M. Li and C. Ma are also with a joint faculty appointment in School of Mechanical Engineering, Shanghai Jiao Tong University.

physical limitations, the ALD-based control is the best for the battery-ultracapacitor HESSs. However, in real applications, besides the physical limitations, it is very difficult, if not impossible, to exactly know the future load demand in advance which indeed significantly limits the applicability of the ALD-based control.

This paper proposes a control approach comparable to the ideal ALD-based control in terms of its performance, but without using exact pre-knowledge of the future load demand. The battery and UC packs are first modeled as two independent but related agents using the NetLogo environment. The agent of the battery pack aims to extend its cycle-life, while the agent of the UC pack works to improve the energy efficiency of the HESS. The different preferences of two agents are represented by their utility functions respectively. This utility function-based control is carried out by solving a multi-objective optimization problem once off-line and then updating the solution in real time. This global optimal solution is then obtained by using Karush-Kuhn-Tucker (KKT) conditions. Finally, both the NetLogo-based simulation and experimental results validate the theoretical analysis.

II. SYSTEM CONFIGURATION AND MODELING

Using a single DC-DC converter, two semi-active topologies are possible for the target HESS, namely capacitor semi-active and battery semi-active hybrids [25]. In the capacitor semi-active hybrid, the DC-DC converter connects the UC pack and the load, while in the battery semi-active hybrid the DC-DC converter is placed between the battery pack and the load as shown in Fig. 1. The capacitor semi-active is advantageous in terms of the capability of fully utilizing the UC pack. The variation/ripple of the DC link voltage is also small due to the fact that batteries usually have a flat voltage profile. However, the DC-DC converter used in this topology needs to have a considerable rating and must be designed according to the peak power. The advantage of the battery semi-active hybrid is that it is capable of enforcing the battery to work at the point close to the average power/current, therefore allows potential improvement in battery performance in terms of cycle-life and energy efficiency [24], [25]. In addition, the voltage matching between the battery pack and the load is not required any more. The DC-DC converter rating is also much lower than that in the capacitor semi-active topology [23], [25]. The main disadvantage of the battery semi-active topology is the variation of the DC link voltage during UC charging/discharging. This may lead to a very large capacitance value and limit the usage of the UC energy. In the following discussion, a battery semi-active HESS is used as an example to apply the utility function-based control. In this topology, the variation of the battery current can be directly controlled for extending the battery cycle life. Meanwhile, as a general approach, the proposed control method can be modified and extended for its applications in the capacitor semi-active HESS and other more complex hybrid energy systems.

Figure 2 shows the experimental setup of the battery-ultracapacitor HESS discussed in this paper. This HESS employs the battery semi-active topology. The power supply and

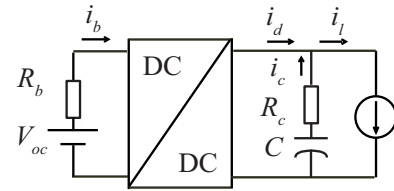
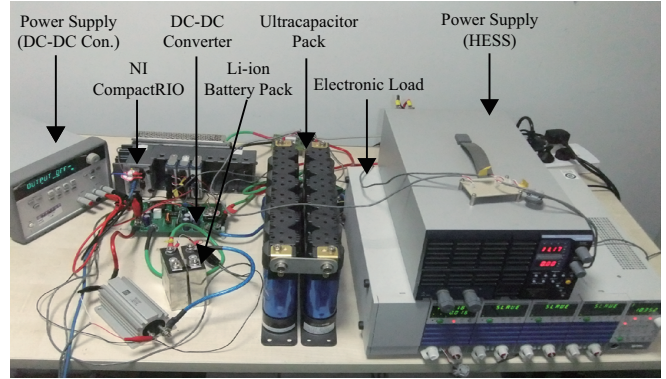
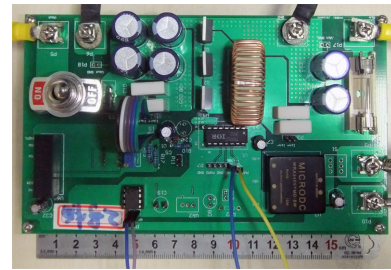


Fig. 1. The topology of the battery semi-active HESS.



(a)



(b)

Fig. 2. Experimental battery semi-active HESS. (a) System configuration. (b) DC-DC converter.

the electronic load are controlled to emulate charging and discharging currents, respectively. The boost DC-DC converter is designed and fabricated in house with an overall efficiency being more than 90%. The Data Acquisition (DAQ) system used is the CompactRIO platform from National Instruments (NI).

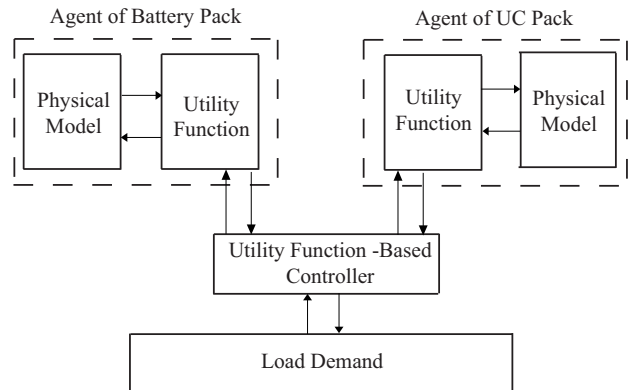


Fig. 3. The architecture of agents in NetLogo.

In order to represent the different characteristics of the battery and UC packs and their interaction in the HESS, a multi-agent based modeling and programming environment, NetLogo, is used. A multi-agent system is defined as a computerized system that is composed of multiple interacting agents within an environment [26], [27]. In the multi-agent system, each agent is independent with different goals or preferences. The purpose is to find out a rule among agents which can lead to a compromised solution that balances the different goals of the agents. NetLogo is an open-source software that has been world-widely used for modeling complex systems evolving over time [28]. It is the basic simulation environment in this paper under which all the simulation models and algorithm are applied. Following the definition of the multi-agent system, here in NetLogo, the battery and UC packs are modeled as two independent but related agents, as shown in Fig. 3. At each control instant, two agents first evaluate their own utility functions according to the interactions between their physical models and the load demand. The utility function here quantifies the satisfaction level of an individual agent for a certain load distribution between the two agents. Based on their respective utility functions or preferences, they work collaboratively and synergically to contribute their own load currents following the determined rule that is implemented by the proposed utility function-based control. Note that other tools can also be used to perform the modeling and simulation of the battery semi-active HESS such as Petri nets, neural networks, and the conventional modeling using physical models [29], [30]. Here the multi-agent based modeling and its environment NetLogo are chosen for reference implementation and validation because they can be easily extended to describe more complex hybrid energy systems, i.e., using more agents to represent newly added devices. In NetLogo, hundreds of agents can be easily created simultaneously and all agents can operate independently [28]. This advantage of NetLogo makes it possible to explore both the individual-level behavior of multiple devices and the system-level patterns that emerge from their interaction. Thus NetLogo is an efficient modeling and simulation environment here to facilitate the agent-based modeling and the utility function-based control, as discussed in the introduction section.

The entire HESS model and the control loop are shown in Fig. 4. The parameters of the HESS model are listed in Tab. I. In the model of the battery pack, V_{oc} is the open circuit voltage and R_b is the internal resistance [31]. Two RC networks with different time constants,

$$\tau_s = R_{t,s}C_{t,s} \text{ and } \tau_m = R_{t,m}C_{t,m} \quad (1)$$

are used to model battery transient voltage responses in second and minute ranges, respectively [32]. Parameters of the battery pack, V_{oc} and R_b , are obtained by using a fast averaging method, and represented by six-ordered polynomial functions [33],

$$V_{oc} = a_{ocv,0} + a_{ocv,1}x + a_{ocv,2}x^2 + \dots + a_{ocv,6}x^6, \quad (2)$$

$$R_b = a_{r,0} + a_{r,1}x + a_{r,2}x^2 + \dots + a_{r,6}x^6, \quad (3)$$

where x is the specific state-of-charge (SOC) of the battery pack. In the model of the UC pack (the bottom block in Fig. 4),

TABLE I
PARAMETERS OF THE HESS MODEL

| Li-ion Battery Pack | | Two cells (Series) | |
|---------------------|-----------------|----------------------|-----------------|
| $a_{ocv,0}$ | 2.30 | $a_{ocv,1}$ | 15.96 |
| $a_{ocv,2}$ | -99.35 | $a_{ocv,3}$ | 295.20 |
| $a_{ocv,4}$ | -446.49 | $a_{ocv,5}$ | 331.41 |
| $a_{ocv,6}$ | -95.56 | $a_{r,0}$ | 0.02 |
| $a_{r,1}$ | -0.24 | $a_{r,2}$ | 1.69 |
| $a_{r,3}$ | -5.66 | $a_{r,4}$ | 9.67 |
| $a_{r,5}$ | -8.13 | $a_{r,6}$ | 2.67 |
| $R_{t,s}$ | 5.60 m Ω | $C_{t,s}$ | 12200 F |
| $R_{t,m}$ | 2.87 m Ω | $C_{t,m}$ | 453000 F |
| UC Pack | | Eight cells (Series) | |
| C | 1760 F | $R_{c,s}$ | 2.50 m Ω |
| $R_{c,l}$ | 3 k Ω | | |
| DC-DC Converter | | Efficiency: > 90% | |
| R_L | 100 m Ω | L | 200 μ H |
| R_{mos} | 5 m Ω | R_{D1} | 12 m Ω |
| V_F | 0.26 V | C_{out} | 2 mF |

C is the capacitance, $R_{c,s}$ is the internal resistance of the UC pack, and $R_{c,l}$ is used to model the leak current [34]. Parameters of the UC pack are obtained by using pulsed current test [35]. A current-mode controlled boost converter is employed in the HESS. The controller determines the reference current of the battery pack i_b^* based on three feedback signals, the current of the battery pack i_b , load current i_l , and the voltage of the UC pack v_c . For the parameters of the DC-DC converter in Tab. I, R_L is the equivalent series resistance of the inductor L ; R_{mos} is the on-resistance of the MOSFET switch S_{mos} ; R_{D1} and V_F are the resistance and the voltage drop of the diode D_1 , respectively; C_{out} is the capacitance of the output capacitor.

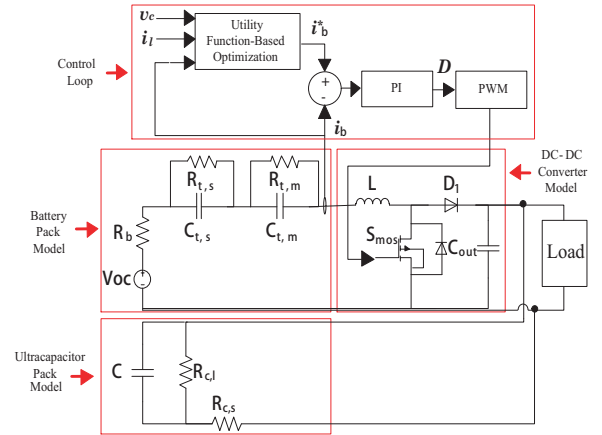


Fig. 4. The HESS model and control loop.

III. DEFINITION OF UTILITY FUNCTIONS

There are two major objectives for the control of the HESS discussed in this paper. The first one is to minimize the variation of the battery current in order to extend the cycle-life of the battery pack. The second one is to minimize the difference between the present UC energy level and its initial level, taking the consideration that the UC pack is only a temporary energy source. Those two objectives can be represented by the utility functions of two agents working

collaboratively in NetLogo, i.e., the respective preferences of the battery and UC packs. Here one utility function quantifies how much benefit one energy storage device could obtain if it provides certain energy at a particular time [36]. The preference of the battery pack is the extension of its cycle-life. It relates to two factors, the amplitude and variation rate of the battery current i_b [21]. On the other hand, the preference of the UC pack is to minimize the difference between its present and initial energy levels. Quadratic functions are used here to represent those utility functions, which achieve their maximum values when the preferences are met [36]. The utility functions of the battery and UC packs are discussed as follows.

A. Battery Pack

The utility function of the battery pack, u_b , is equivalent to the utility of the battery cycle-life in this paper:

$$u_b = w_{b,ave}u_{b,ave} + w_{b,dif}u_{b,dif}, \quad (4)$$

where u_b contains two parts, $u_{b,ave}$ and $u_{b,dif}$. The aim of $u_{b,ave}$ is to minimize the amplitude of the battery current while the aim of $u_{b,dif}$ is to minimize the variation rate of the current. $w_{b,ave}$ and $w_{b,dif}$ are weight coefficients for $u_{b,ave}$ and $u_{b,dif}$, respectively. Determination of $w_{b,ave}$ and $w_{b,dif}$ is discussed in the following section. $u_{b,ave}$ and $u_{b,dif}$ are defined as

$$u_{b,ave} = 1 - a(i_b - i_{b,ave})^2, \quad (5)$$

$$u_{b,dif} = 1 - b(i_b - i_{b,l})^2, \quad (6)$$

respectively. Here $i_{b,ave}$ is the average current of the battery pack from the beginning to the current control instant. $i_{b,l}$ is the current of the battery pack at the last control instant. The coefficient a can be calculated using Eq. (7). The equation is designed to normalize the value of $u_{b,ave}$. When i_b reaches its maximum value $I_{b,max}$, $u_{b,ave}$ is equal to zero. Similarly, the coefficient b normalizes the value of $u_{b,dif}$ to be zero when the variation of i_b comes to its maximum threshold, $Max(|i_b - i_{b,l}|)$, within a single sampling interval [refer to Eq. (8)]. This threshold should be specified based on the performance and design requirements of the target HESS.

$$a = \frac{1}{(i_{b,max} - i_{b,ave})^2} \quad (7)$$

$$b = \frac{1}{[Max(|i_b - i_{b,l}|)]^2} \quad (8)$$

B. Ultracapacitor Pack

The utility function of the UC pack u_c can be represented as an utility of its stored energy $u_{c,eng}$ with a weight coefficient $w_{c,eng}$:

$$u_c = w_{c,eng}[1 - c(i_c - i_{c,fit})^2], \quad (9)$$

where

$$c = \frac{1}{(I_{c,max} - i_{c,fit})^2}. \quad (10)$$

The larger the utility values, the closer the current of the UC pack i_c to a designed current value $i_{c,fit}$, whose purpose is to bring the UC energy level back to its initial level in the

most convenient manner (its formulation will be defined later in this section). c is calculated in the same way as a and b in Eqs. (7) and (8). $I_{c,max}$ is the maximum permissible current of the UC pack.

UCs usually work as "energy buffers" in many HESSs, and for an UC pack, its stored energy is

$$e_c = \frac{1}{2}Cv_c^2, \quad (11)$$

where C is the capacitance and v_c is the voltage of the UC pack. Considering the equal chance of charging and discharging of an UC pack in a dynamic environment, the UC pack's initial voltage $V_{c,ini}$ could be specified as

$$V_{c,ini} = \sqrt{\frac{V_{c,max}^2 + V_{c,min}^2}{2}}, \quad (12)$$

i.e., a 50% initial SOC. $V_{c,max}$ and $V_{c,min}$ are the maximum and minimum voltages of the UC pack, respectively. Thus to control the voltage of the UC pack, its reference current $i_{c,fit}$ is designed by scaling $I_{c,max}$ based on the energy difference between the present and initial levels:

$$i_{c,fit} = \left(2 \frac{v_c^2 - V_{c,min}^2}{V_{c,max}^2 - V_{c,min}^2} - 1\right) I_{c,max}. \quad (13)$$

In this way, when i_c is closer to $i_{c,fit}$, the UC pack is properly charged/discharged to reach its initial level of the stored energy. Here a positive current means discharging, and vice versa. In the utility function Eq. (9), the larger the difference between the present and initial energy levels of the UC pack is, the larger i_c should be (within a range from $-I_{c,max}$ to $I_{c,max}$).

IV. OPTIMIZATION PROBLEM

A. Problem Formulation

The utility functions of the battery and UC packs can be directly used as objective functions (OBJ) of the optimization problem that should be optimized simultaneously,

$$\text{OBJ}_1 : f_{min} = -u_b, \quad (14)$$

$$\text{OBJ}_2 : f_{min} = -u_c. \quad (15)$$

In order to transform this multi-objective optimization problem into a single-objective optimization problem (so that one global optimal solution can be obtained), the weighted-sum method is used. There are other alternative multi-objective optimization approaches, such as compromise programming, physical programming and evolutionary algorithms, in the literature [37], [38]. Here the weight-sum method is chosen because it can provide one analytical solution, instead of numerical or heuristic ones, for the following real-time implementation (in the implementation, only one global optimal solution is necessary). The entire objective function can be formulated as follows,

$$\text{OBJ} : f_{min} = -w_{b,ave}u_{b,ave} - w_{b,dif}u_{b,dif} - w_{c,eng}u_c, \quad (16)$$

subject to

$$0 \leq (w_{b,ave}, w_{b,dif}, w_{c,eng}) \leq 1, \quad (17)$$

where $w_{b,ave}$, $w_{b,dif}$, and $w_{c,eng}$ are three weight coefficients for the respective utility functions. The selection of those coefficients is discussed in Section IV-C. Other constraints are also necessary to make this optimization problem practically feasible. One important constraint is to guarantee that the sum of the currents from the battery and UC packs is equal to the load current i_l , i.e.,

$$i_c + i_b(1 - D) - i_l = 0 \quad (18)$$

where D is the duty cycle of the boost DC-DC converter.

Two design variables of the optimization problem are $x_1 = i_b$ and $x_2 = i_c$. The optimization problem can then be formulated as follows,

$$\begin{aligned} \text{Minimize } f(x_1, x_2) = & -w_{b,ave}[1 - a(x_1 - i_{b,ave})^2] \\ & -w_{b,dif}[1 - b(x_1 - i_{b,l})^2] \\ & -w_{c,eng}[1 - c(x_2 - i_{c,fit})^2] \end{aligned} \quad (19)$$

subject to

$$x_2 + x_1(1 - D) - i_l = 0, \quad (20)$$

$$w_{b,ave} + w_{b,dif} + w_{c,eng} = 1, \quad (21)$$

$$0 \leq (w_{b,ave}, w_{b,dif}, w_{c,eng}) \leq 1. \quad (22)$$

B. Karush-Kuhn-Tucker Conditions

The Karush-Kuhn-Tucker (KKT) conditions are used here to solve the above nonlinear optimization problem theoretically [38], [39]. The objective function and the constraints in Eqs. (19)-(22) can be put into the Lagrangian function L which is depending on x_1 , x_2 , v .

$$\begin{aligned} L = & -w_{b,ave}[1 - a(x_1 - i_{b,ave})^2] - w_{b,dif}[1 - b(x_1 - i_{b,l})^2] \\ & - w_{c,eng}[1 - c(x_2 - i_{c,fit})^2] + v[x_1(1 - D) + x_2 - i_l], \end{aligned} \quad (23)$$

Let

$$\begin{aligned} \frac{\partial L}{\partial x_1} = & 2aw_{b,ave}(x_1 - i_{b,ave}) + 2bw_{b,dif}(x_1 - i_{b,l}) \\ & + (1 - D)v = 0, \end{aligned} \quad (24)$$

$$\frac{\partial L}{\partial x_2} = 2w_{c,eng}c(x_2 - i_{c,fit}) + v = 0, \quad (25)$$

$$\frac{\partial L}{\partial v} = x_1(1 - D) + x_2 - i_l = 0, \quad (26)$$

the KKT candidate point is then solved as

$$x_1 = \frac{aw_{b,ave}i_{b,ave} + bw_{b,dif}i_{b,l} + cw_{c,eng}(1-D)(i_l - i_{c,fit})}{aw_{b,ave} + bw_{b,dif} + c(1-D)w_{c,eng}}, \quad (27)$$

$$x_2 = i_l - (1 - D)x_1, \quad (28)$$

$$v = 2cw_{c,eng}[(1 - D)x_1 + i_{c,fit} - i_l]. \quad (29)$$

The Hessian of the Lagrangian function is

$$\nabla^2 L = \begin{bmatrix} \frac{\partial^2 L}{\partial x_1^2} & \frac{\partial^2 L}{\partial x_1 \partial x_2} \\ \frac{\partial^2 L}{\partial x_1 \partial x_2} & \frac{\partial^2 L}{\partial x_2^2} \end{bmatrix} \quad (30)$$

$$= \begin{bmatrix} 2aw_{b,ave} + 2bw_{b,dif} & 0 \\ 0 & 2cw_{c,eng} \end{bmatrix}, \quad (31)$$

which is always positive definite. Thus the solution in Eqs. (27) and (28) is a global minimum point that determines an optimal distribution of the current between the battery and UC packs. Notice that this single-objective optimization problem is only solved once off-line before the control procedure, and the solution only needs to be updated at every control instant.

In real applications, there are also physical box constraints on the upper and lower bounds of the currents of the battery and UC packs,

$$-x_1 \leq 0, \quad (32)$$

$$x_1 - I_{b,max} \leq 0, \quad (33)$$

$$-x_2 - I_{c,max} \leq 0, \quad (34)$$

$$x_2 - I_{c,max} \leq 0. \quad (35)$$

Notice that the optimization problem defined in Eqs. (19)-(22) is still a convex problem defined on this bounded box and the global minimum solution from Eqs. (27)(28) still holds if it is within the physical box. However, if it is located out of the above box, the local optimal solution is simply located on the boundary of the box.

C. Determination of Weight Coefficients

As shown in Eq. (27) and (28), the solution to the optimization problem is symbolically represented by a function of the weight coefficients. As long as the values of those coefficients are determined, the optimal solution can be updated at each control instant. The coefficients should be determined as the values that can provide the best balance between the different preferences of the battery and UC packs, i.e., the knee point of the Pareto set discussed below [40].

Among those weight coefficients, $w_{c,eng}$ can be first calculated in an adaptive manner,

$$w_{c,eng} = w_{c,min} + \frac{1 - w_{c,min}}{V_{c,ini}^2 - V_{c,min}^2} |V_{c,ini}^2 - v_c^2|. \quad (36)$$

This function is used to make sure that $w_{c,eng}$ goes to $w_{c,min}$ when the energy stored in the UC pack equals to its initial energy level, and it becomes one when the UC pack is fully charged or discharged, i.e., $w_{c,min}$ is the lowest value of $w_{c,eng}$.

$w_{c,min}$, $w_{b,ave}$, and $w_{b,dif}$ can be determined based on a targeted test cycle such as JC08 driving cycle (the Japanese urban test cycle representing congested city driving conditions) [41], [42]. JC08 here serves as an example of a realistic power profile. Note that the approach discussed below itself is a general one which is not limited to any specific application. For any other targeted test cycles, the weight coefficients can be determined following the same procedure. Figure 5 shows the velocity and power profiles of JC08, in which the maximum speed is 81.6 km/h and the average speed is 24.4 km/h. The power profile of the JC08 driving cycle is scaled down to match the power capability of the experimental HESS described in Section II.

As shown in the objective function Eq. (19), $w_{b,ave}$ emphasizes the long-term variation of the battery current, $w_{b,dif}$ represents the influence of a short-term one, and $w_{c,eng}$ (or $w_{c,min}$) controls the convergence speed of the current of the

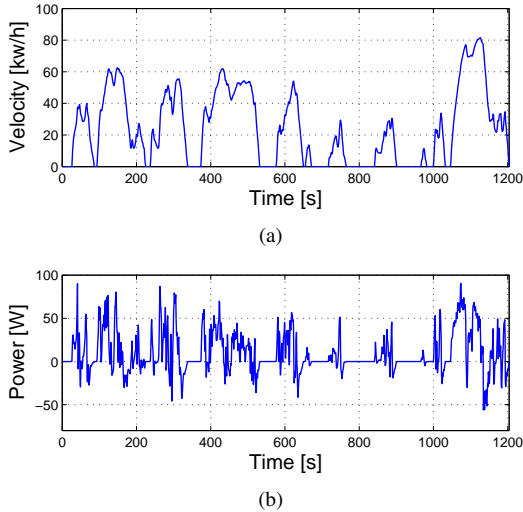


Fig. 5. Velocity and power profiles for the JC08 driving cycle. (a) Velocity profile. (b) Power profile.

battery pack to the average load current. Various combinations of $w_{c,min}$, $w_{b,ave}$ and $w_{b,dif}$ are applied to calculate the variation of the average battery current sampled in: 1) large (10 minutes) and 2) short (0.35 second) time intervals, and 3) the average energy stored in the UC pack, respectively. 0.35 second is the sampling interval of the host PC in the experimental HESS. The tradeoff relationship among three weights can be represented by the so-called Pareto set [see Fig. 6] [38]. In the figure, x axis is the normalized average energy stored in the UC pack; y and z axes are the normalized short and long-term variations of the battery current, respectively. In the normalization, “0” corresponds to the minimum of a variable, and “1” is the maximum. The knee point with the combination of

$$w_{c,min} = 0.6, \quad \frac{w_{b,ave}}{w_{b,dif}} = \frac{1}{4}, \quad (37)$$

gives the most satisfactory solution. This knee point is closest to (0,0,0), on which the x axis is the normalized initial energy of the UC pack, the y and z axes are the normalized lowest short-term and long-term current variations. Any deviation from the knee point favors one or two of the three criteria, but sacrifices the other more. The three weights, $w_{b,ave}$, $w_{b,dif}$, and $w_{c,eng}$, can be finally determined using the relationships described in Eqs. (22), (36) and (37).

The influences of $w_{b,ave}$, $w_{b,dif}$, and $w_{c,eng}$ are illustrated in Fig. 7, where the JC08 driving cycle runs eight times. In accordance with their definitions, $w_{b,ave}$ minimizes the difference between i_b and $i_{b,ave}$, i.e., suppressing the amplitude of i_b ; $w_{b,dif}$ affects the distribution of the dynamic load current (the smaller $w_{b,dif}$ is, the more dynamic current the battery pack provides); and $w_{c,eng}$ controls the convergence speed of i_b to an average value, which is $\frac{1}{1-D}$ times of the average load current in the test cycle. Again D is the duty cycle of the DC-DC converter.

Finally, for the current example application in electric vehicles (EVs), additional constraints such as the allowable range of DC link voltage have to be considered. Because of the

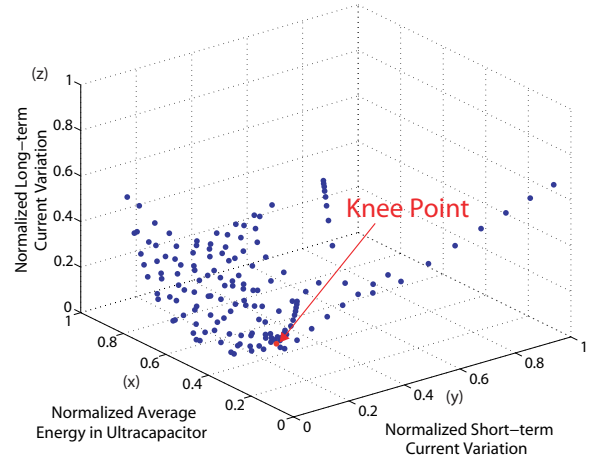
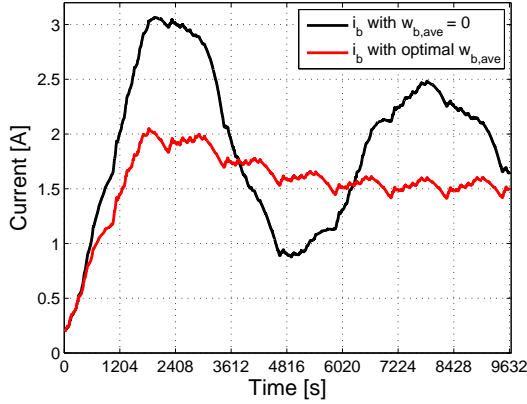


Fig. 6. The Pareto set.

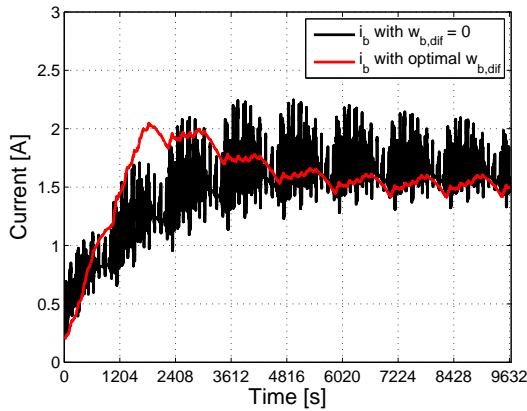
battery semi-active topology used, the DC link voltage is equal to the UC voltage. Considering this constraint, a larger $w_{c,eng}$, the weight coefficient to favor the storage energy in UC pack and thus the UC voltage, can be used. As shown in Fig. 8(a), a large $w_{c,eng}$ such as 0.9 enables a faster convergence of the UC voltage, i.e., the DC link voltage. Thus the low UC voltage in the first two cycles can be improved. However, due to the limitation of the semi-active topology, a tradeoff relationship exists among the weight coefficients. The variation of the battery current also becomes greater with the larger $w_{c,eng}$ [see Fig. 8(b)]. In real applications, a lower boundary of $w_{c,eng}$ should be determined according to specific limitations on the allowable range of DC link voltage. Besides, for the sake of simplicity of this work the initial value of the average battery current, $i_{b,ave}$, is set to be zero. The variation of the DC link voltage can also be improved by having a properly selected initial $i_{b,ave}$, as discussed in the last paragraph of Section V. It can be seen that an adaptive mechanism can be included to automatically tune the weight coefficients such as the rule-based approaches [18]. This effort is considered as a part of the future work.

D. Real time implementation

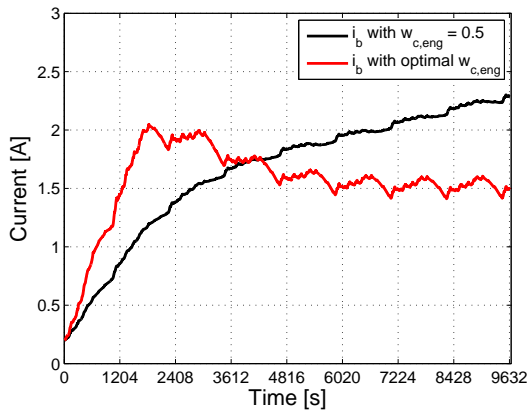
The solution in Eqs. (27) and (28) is a global optimal solution to the optimization problem with only two variables and three parameters. Those parameters are $i_{b,l}$ (the last current of the battery pack), v_c (the voltage of the UC pack), and i_l (the current load demand). Obviously, there is no need to solve the optimization problem at each control instant. This optimal solution only needs to be updated using the newest parameter values at each instant. Also, since the problem is solved by KKT conditions theoretically, the computational effort of this optimization problem can be even neglected. The above utility function-based control is obviously fast enough to be directly implemented in real time. At the same time, delays exist in any practical control system (during sensing, conversions between analog and digital signals, computation, actuating, etc.). They may affect the convergence speed of the battery current i_b , and such the dynamic response of the UC stored energy e_c . Because in the HESS, the battery pack is a primary



(a)



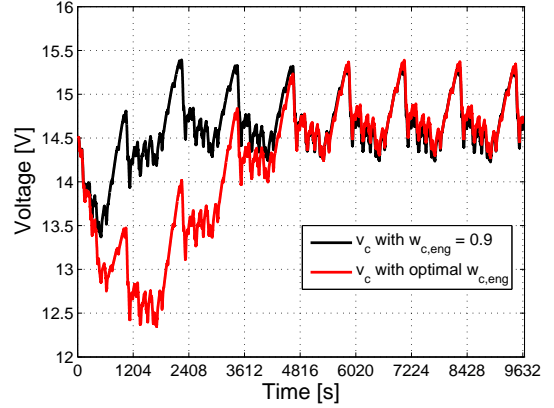
(b)



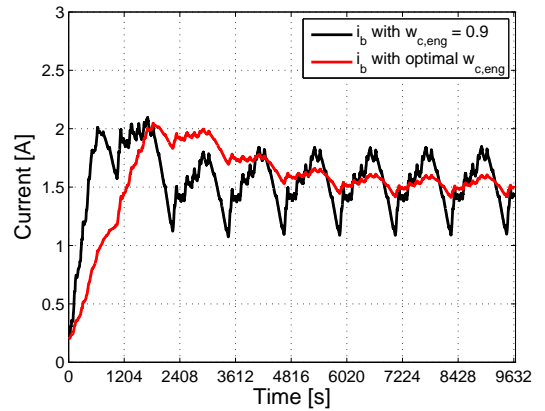
(c)

Fig. 7. Influences of the weight coefficients. (a) $w_{b,ave}$. (b) $w_{b,dif}$. (c) $w_{c,eng}$.

energy source. The control here emphasizes the convergence of the battery current, namely the long-term behavior of the battery pack. In this regard, the control performance is insensitive to the certain delays. In the following simulation and experiments, a relatively large sampling interval, 0.35 second, is applied according to control hardware performance. The results validate the real-time implementation of the utility function-based control.



(a)



(b)

Fig. 8. Influences of the constraint on the allowable range of DC link voltage. (a) Voltages of the UC pack. (b) Currents of the battery pack.

V. SIMULATION RESULTS

The JC08 driving cycle has been repeated eight times in order to decrease the SOC of the battery pack from 80% to 40%, which will last 160 minutes. Although a specific test cycle is used here as an example, its properties such as the average current are unknown for the controller, i.e., the exact pre-knowledge of the driving cycle is not required. The proposed control method itself is applicable for any other random driving cycles.

As defined in Eqs. (38)-(40), the average battery current $I_{b,ave}$, the root mean square (RMS) of the battery current variation $I_{b,var}$, and the average energy stored in the UC pack $E_{c,ave}$, are used as the evaluation criteria:

$$I_{b,ave} = \frac{\sum i_b}{N}, \quad (38)$$

$$I_{b,var} = \sqrt{\frac{\sum (i_b - i_{b,l})^2}{N}}, \quad (39)$$

$$E_{c,ave} = \frac{\sum \frac{1}{2} C v_c^2}{N}, \quad (40)$$

where N is the total number of the control instants. While it is known to be difficult to quantitatively evaluate the cycle-life of batteries, $I_{b,var}$ could serve here as a criterion to indicate

the improvement on the cycle-life [16], [17], [21], because the smaller $I_{b,var}$, the smaller the change in the battery current, and thus the longer the battery cycle life.

Results of the two control methods, the proposed utility function-based control and the ALD-based control, are summarized in Tab. II. It can be seen that $I_{b,ave}$ in the two methods are quite close, while the difference in $I_{b,var}$ is relatively large because unlike the ALD-based control, the average load current of the test cycle is unknown in the utility function-based method. Figure 9(a) compares the current responses of the battery pack in the two methods. In the subfigure, 1.54 A is the average current in the ALD-based control. The energy stored in the UC pack e_c is shown in Fig. 9(b). Both i_b and e_c converge to the average battery current in the ALD-based control and the initial energy stored in the UC pack, respectively. The results show that the utility function-based method provides a comparable control performance to the ALD-based control. However, this method does not need exact pre-knowledge of the test driving cycle. The voltages of the UC pack are shown in Fig. 9(c). The zero initial value of $i_{b,ave}$ here causes the large variation of the UC voltage in the beginning, as discussed later.

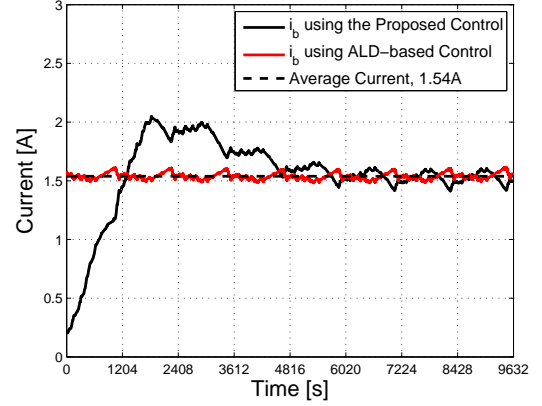
TABLE II
COMPARISON OF SIMULATION RESULTS

| Control | $I_{b,ave}$ | $I_{b,var}$ | $E_{c,ave}$ |
|--------------------|-------------|------------------------|-------------|
| ALD-based | 1.54 A | $1.46 \cdot 10^{-4}$ A | 12021.26 J |
| Utility fun.-based | 1.55 A | $3.52 \cdot 10^{-4}$ A | 11270.79 J |

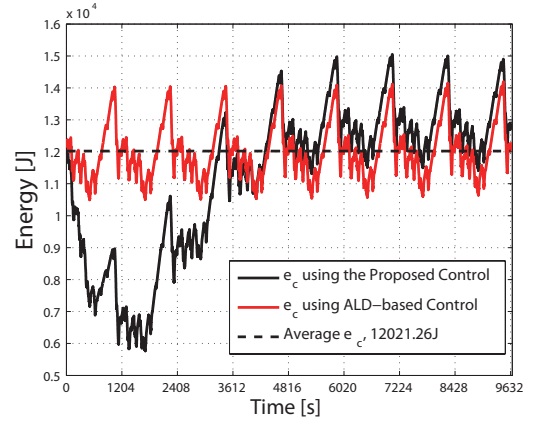
Figure 10 shows the current of the DC-DC converter, i_d , the current of the UC pack, i_c , and the load current, i_l . It shows that the current of the battery pack (through the DC-DC converter) covers the average load current, the UC pack covers the dynamic current, and the sum of them is the load current.

The initial value of $i_{b,ave}$ (the average current of the battery pack so far) plays an important role in this work. In the simulation, the initial $i_{b,ave}$ is set to be zero which causes a large current variation in the battery pack during the first 40 minutes, as shown in Fig. 11(a). After that, $i_{b,ave}$ converges to the average current of the test cycle up to the present control instant and thus the variation in the last 40 minutes becomes much smaller [see Fig.11(b)]. The initial value of $i_{b,ave}$ also influences the variation of the UC voltage, i.e., the DC link voltage in the battery semi-active HESS. As shown in Fig. 12(a), the UC voltage can drop to as low as about 12.5 V in the first two test cycles. While with the update of $i_{b,ave}$, the variation range of the UC voltage is significantly decreased to around 14 to 15.4 V [see Fig. 12(b)]. This result shows that the variation of the DC link voltage can also be improved with a proper initial value of $i_{b,ave}$ instead of zero.

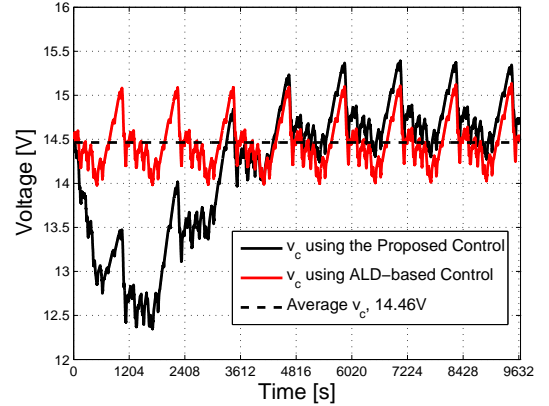
In addition, as shown in Fig. 13, the current of the battery pack converges more quickly as the window size becomes larger. This phenomenon can be understood as that if the window size is larger, $i_{b,ave}$ will change more smoothly. Therefore the window size in this simulation is selected as from the time zero to the present control instant, i.e., $i_{b,ave}$ is calculated using all the sampled currents of the battery pack



(a)



(b)



(c)

Fig. 9. Responses in eight test cycles. (a) Currents of the battery pack. (b) Energy stored in the UC pack. (c) Voltages of the UC pack.

so far.

VI. EXPERIMENTAL VERIFICATION

Figure 14 and Tab. III show the block-diagram and specifications of the experimental HESS system [see Fig. 2]. Again the power supply and the electronic load are controlled by the PC running NI Labview. They are combined together to emulate the JC08 test cycle, i.e., the charging and discharging

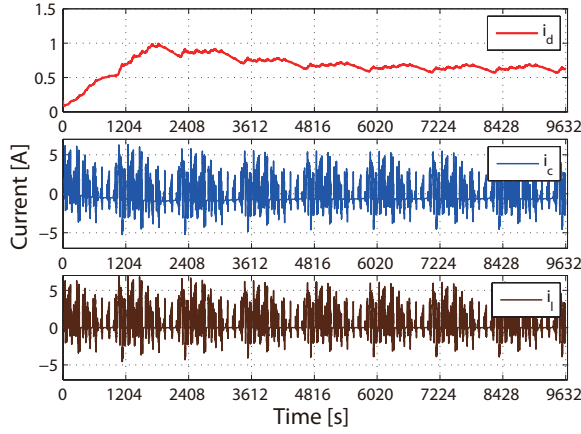
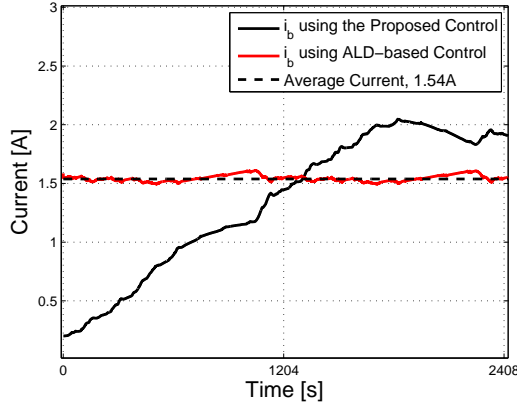
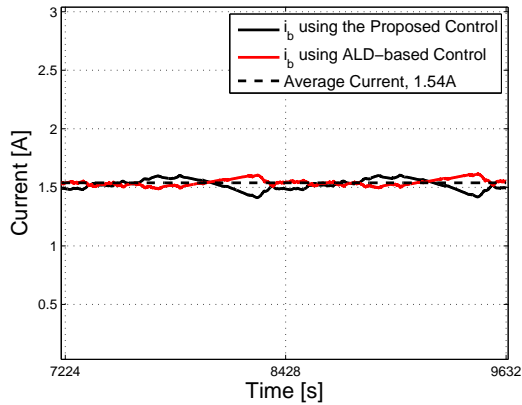


Fig. 10. Overall current responses in simulation.



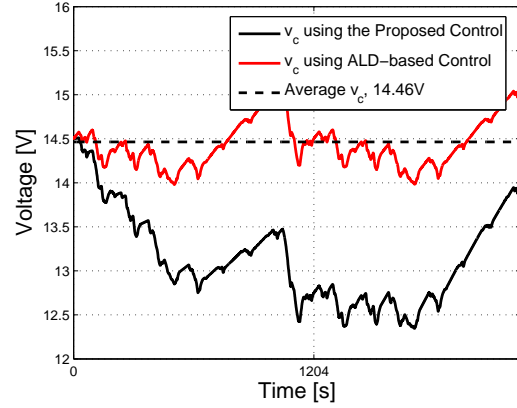
(a)



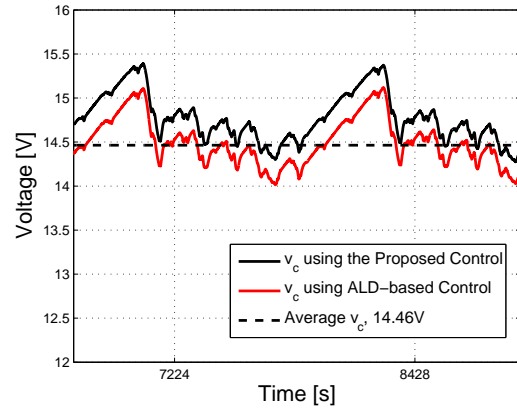
(b)

Fig. 11. Influence of the initial $i_{b,ave}$. (a) First two test cycles. (b) Last two test cycles.

currents, i_{ch} and i_{dis} . The NI CompactRIO system collects data including the voltage of the battery pack v_b , the voltage of the UC pack v_c , the current of the battery pack i_b , the output current of the DC-DC converter i_{dcdc} , and load current i_l . Two 0.01Ω high-accuracy sampling resistors, R_{s1} and R_{s3} are used to measure i_b and i_l . I_{dcdc} is measured using a 0.1Ω sampling resistor R_{s2} (two 0.2Ω high-accuracy resistors



(a)

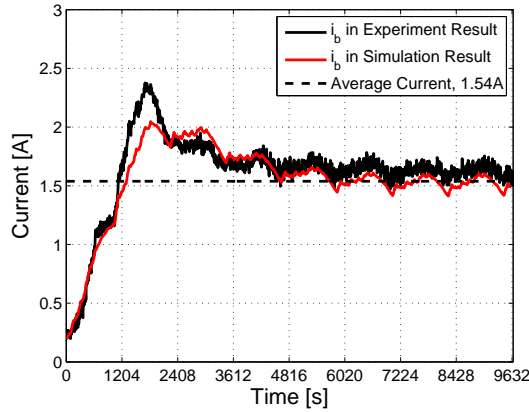


(b)

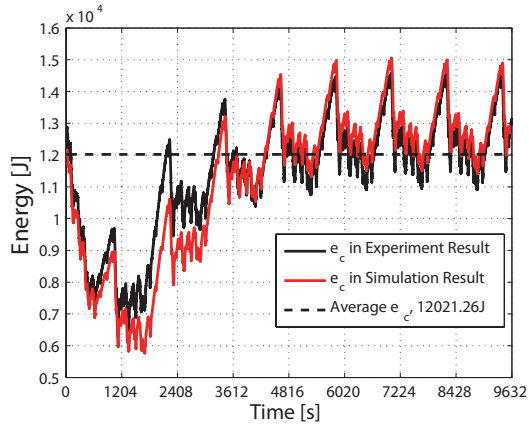
Fig. 12. Influence of the initial $i_{b,ave}$ on the voltage of the UC pack. (a) First two test cycles. (b) Last two test cycles.

connected in parallel). The boost DC-DC converter is also controlled by the NI compactRIO system. The optimal solution in Eqs. (27)(28) is updated in the host PC at every control instant with a sampling interval of 0.35 second. The reference command of i_b , i_b^* , is sent to the NI compactRIO controller from the host PC. In the LabVIEW program, each energy storage device (i.e., the battery and UC packs here) has its own independent while loop. As mentioned in Section III, those two while loops are run based on their respective utility functions or preferences. The while loop of the battery pack works to minimize the variation of the battery current for extending the cycle life of the battery pack; while the objective of the while loop for the UC pack is to minimize the difference between the present UC energy level and its initial level (because the UC pack is only a temporary energy source.)

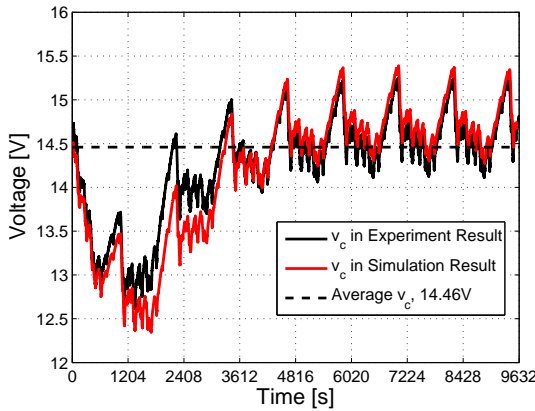
As shown in Fig. 15, the experimental results match the simulation results closely. This proves the correctness of the real-time implementation of the proposed control. The current of the battery pack successfully converges to the average current. The small variations between the simulation and experimental results are mainly caused by the extra energy losses in real circuits such as from the DC-DC converter, current sampling resistors, and wires. This leads to different



(a)

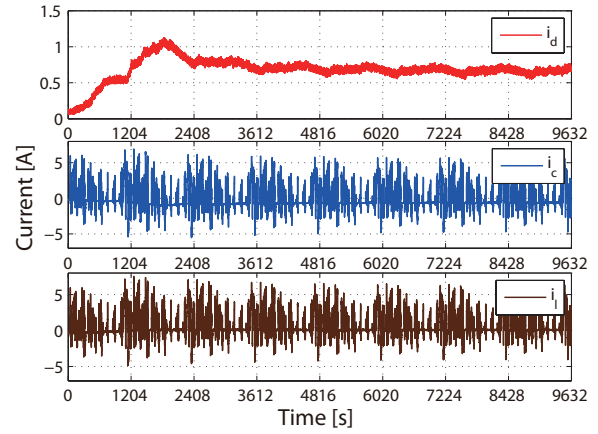


(b)

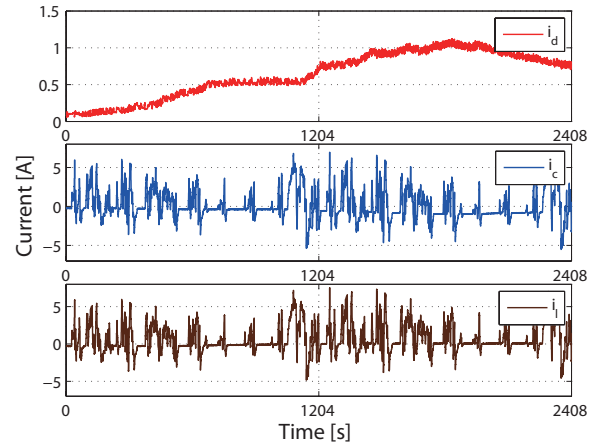


(c)

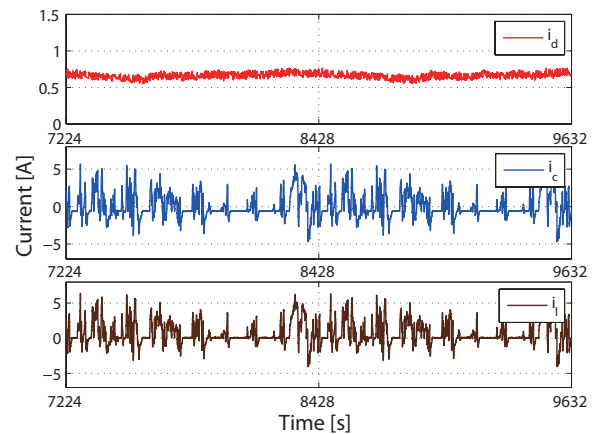
Fig. 15. Comparisons between the experimental and simulation results (eight test cycles in total). (a) The current of the battery pack. (b) The energy stored in the UC pack. (c) Voltages of the UC pack.



(a)



(b)



(c)

Fig. 16. Overall current responses in experiments. (a) Eight test cycles. (b) First two test cycles. (c) Last two test cycles.

[7] A. Burke and M. Miller, "The power capability of ultracapacitors and lithium batteries for electric and hybrid vehicle applications," *Journal of Power Sources*, vol. 196, no. 1, pp. 514–522, 2011.
 [8] A. Burke, "Ultracapacitors: why, how, and where is the technology," *Journal of Power Sources*, vol. 91, no. 1, pp. 37–50, 2000.
 [9] P. Thounthong, S. Raël, and B. Davat, "Control strategy of fuel cell and supercapacitors association for a distributed generation system," *IEEE Trans. Ind. Electron.*, vol. 54, no. 6, pp. 3225–3233, 2007.
 [10] T. Azib, O. Bethoux, G. Remy, C. Marchand, and E. Berthelot, "An innovative control strategy of a single converter for hybrid fuel

cell/supercapacitor power source," *IEEE Trans. Ind. Electron.*, vol. 57, no. 12, pp. 4024–4031, 2010.
 [11] Z. Amjadi and S. S. Williamson, "Power-electronics-based solutions for plug-in hybrid electric vehicle energy storage and management systems," *IEEE Trans. Ind. Electron.*, vol. 57, no. 2, pp. 608–616, 2010.
 [12] J. Moreno, M. E. Ortúzar, and J. W. Dixon, "Energy-management system for a hybrid electric vehicle, using ultracapacitors and neural networks," *IEEE Trans. Ind. Electron.*, vol. 53, no. 2, pp. 614–623, 2006.
 [13] W.-S. Lin and C.-H. Zheng, "Energy management of a fuel cell/ultracapacitor hybrid power system using an adaptive optimal-control method," *Journal of Power Sources*, vol. 196, no. 6, pp. 3280–

- 3289, 2011.
- [14] O. Erdinc, B. Vural, and M. Uzunoglu, "A wavelet-fuzzy logic based energy management strategy for a fuel cell/battery/ultra-capacitor hybrid vehicular power system," *Journal of Power Sources*, vol. 194, no. 1, pp. 369–380, 2009.
- [15] M. Zandi, A. Payman, J.-P. Martin, S. Pierfederici, B. Davat, and F. Meibody-Tabar, "Energy management of a fuel cell/supercapacitor/battery power source for electric vehicular applications," *IEEE Trans. Veh. Technol.*, vol. 60, no. 2, pp. 433–443, 2011.
- [16] S. Dusmez and A. Khaligh, "A supervisory power splitting approach for a new ultracapacitor-battery vehicle deploying two propulsion machines," *IEEE Trans. Ind. Informat.*, vol. 10, no. 3, pp. 1960–1971, 2014.
- [17] J. Shen, S. Dusmez, and A. Khaligh, "Optimization of sizing and battery cycle life in battery/uc hybrid energy storage system for electric vehicle applications," in *IEEE Trans. Ind. Informat.* 2014, DOI:10.1109/TII.2014.2334233.
- [18] W. Zhou, M. Li, H. Yin, and C. Ma, "An adaptive fuzzy logic based energy management strategy for electric vehicles," in *2014 IEEE 23rd International Symposium on Industrial Electronics (ISIE)*, Istanbul, Turkey, June 1-4, 2014, pp. 1778–1783.
- [19] D. Rotenberg, A. Vahidi, and I. Kolmanovsky, "Ultracapacitor assisted powertrains: Modeling, control, sizing, and the impact on fuel economy," *IEEE Trans. Control Syst. Technol.*, vol. 19, no. 3, pp. 576–589, 2011.
- [20] O. Laldin, M. Moshirvaziri, and O. Trescases, "Predictive algorithm for optimizing power flow in hybrid ultracapacitor/battery storage systems for light electric vehicles," *IEEE Trans. Power Electron.*, vol. 28, no. 8, pp. 3882–3895, 2013.
- [21] M.-E. Choi, S.-W. Kim, and S.-W. Seo, "Energy management optimization in a battery/supercapacitor hybrid energy storage system," *IEEE Trans. Smart Grid*, vol. 3, no. 1, pp. 463–472, 2012.
- [22] L. Gao, R. A. Dougal, and S. Liu, "Power enhancement of an actively controlled battery/ultracapacitor hybrid," *IEEE Trans. Power Electron.*, vol. 20, no. 1, pp. 236–243, 2005.
- [23] J. Cao and A. Emadi, "A new battery/ultracapacitor hybrid energy storage system for electric, hybrid, and plug-in hybrid electric vehicles," *IEEE Trans. Power Electron.*, vol. 27, no. 1, pp. 122–132, 2012.
- [24] A. Kuperman, I. Aharon, S. Malki, and A. Kara, "Design of a semi-active battery-ultracapacitor hybrid energy source," *IEEE Trans. Power Electron.*, vol. 28, no. 2, pp. 806–815, 2013.
- [25] A. Kuperman and I. Aharon, "Battery-ultracapacitor hybrids for pulsed current loads: A review," *Renew. Sust. Energy Rev.*, vol. 15, no. 2, pp. 981–992, 2011.
- [26] M. Wooldridge, *An introduction to multiagent systems*. John Wiley & Sons, 2009.
- [27] M. Niazi and A. Hussain, "Agent-based computing for multi-agent systems to agent-based models: a visual survey," *Scientometrics*, vol. 89, no. 2, pp. 479–499, 2011.
- [28] Netlogo [Online] Available: <http://ccl.northwestern.edu/netlogo/>.
- [29] D. Lu, H. Fakhm, T. Zhou, and B. François, "Application of petri nets for the energy management of a photovoltaic based power station including storage units," *Renewable energy*, vol. 35, no. 6, pp. 1117–1124, 2010.
- [30] T. Weigert, Q. Tian, and K. Lian, "State-of-charge prediction of batteries and battery-supercapacitor hybrids using artificial neural networks," *Journal of Power Sources*, vol. 196, no. 8, pp. 4061–4066, 2011.
- [31] M. Chen and G. A. Rincon-Mora, "Accurate electrical battery model capable of predicting runtime and $I-V$ performance," *IEEE Trans. Energy Convers.*, vol. 21, no. 2, pp. 504–511, 2006.
- [32] S. Abu-Sharkh and D. Doerffel, "Rapid test and non-linear model characterisation of solid-state lithium-ion batteries," *Journal of Power Sources*, vol. 130, no. 1, pp. 266–274, 2004.
- [33] R. C. Kroeze and P. T. Krein, "Electrical battery model for use in dynamic electric vehicle simulations," in *IEEE Power Electronics Specialists Conference (PESC'08)*, Rhodes, Greece, June, 2008, pp. 1336–1342.
- [34] M. S. Chan, K. Chau, and C. Chan, "Effective charging method for ultracapacitors," *Journal of Asian Electric Vehicles*, vol. 3, no. 2, pp. 771–776, 2005.
- [35] W. Lajnef, J.-M. Vinassa, O. Briat, S. Azzopardi, and E. Woingard, "Characterization methods and modelling of ultracapacitors for use as peak power sources," *Journal of Power Sources*, vol. 168, no. 2, pp. 553–560, 2007.
- [36] R. T. Clemen and T. Reilly, *Making hard decisions with Decision Tools Suite*. Duxbury, 1999.
- [37] A. Messac and C. A. Mattson, "Generating well-distributed sets of pareto points for engineering design using physical programming," *Optimization and Engineering*, vol. 3, no. 4, pp. 431–450, 2002.

- [38] J. Arora, *Introduction to optimum design*. Academic Press, 2004.
- [39] N. Rahbari-Asr and M. Chow, "Cooperative distributed demand management for community charging of PHEV/PEVs based on KKT conditions and consensus networks," *IEEE Trans. Ind. Informat.*, vol. 10, no. 3, pp. 1907–1916, 2014.
- [40] J. Branke, K. Deb, H. Dierolf, and M. Osswald, "Finding knees in multi-objective optimization," in *Parallel Problem Solving from Nature-PPSN VIII*. Springer, 2004, pp. 722–731.
- [41] K. Kiyota, H. Sugimoto, and A. Chiba, "Comparison of energy consumption of SRM and IPMSM in automotive driving schedules," in *Proc. IEEE Energy Conversion Congress and Exposition (ECCE'12)*, Raleigh, NC, USA, Sep. 2012, pp. 853–860.
- [42] S. Chopra and P. Bauer, "Driving range extension of EV with on-road contactless power transfer-a case study," *IEEE Trans. Ind. Electron.*, vol. 60, no. 1, pp. 329–338, 2013.



He Yin (S'13) received the B.S. degree in the electrical and computer engineering from University of Michigan-Shanghai Jiao Tong University Joint Institute, Shanghai Jiao Tong University, Shanghai, China in 2012. He is currently working toward Ph.D. degree in the same institute.

His research interests include optimization and control of alternative energy systems such as energy storage systems using ultracapacitors and wireless power transfer systems.



Chen Zhao (S'14) received the B.S.E.E. degree from East China University of Science and Technology, Shanghai, China, in 2011. He is currently working toward Ph.D. degree in electrical and computer engineering, University of Michigan-Shanghai Jiao Tong University Joint Institute, Shanghai Jiao Tong University, Shanghai, China.

His research interests include analysis, modeling and control of hybrid energy systems using ultracapacitors.



Mian Li currently is an associate professor in the University of Michigan-Shanghai Jiao Tong University Joint Institute, adjunct associate professor at the school of mechanical Engineering, at Shanghai Jiao Tong University, Shanghai, China. He received his Ph.D. degree from the Department of Mechanical Engineering, University of Maryland at College Park in December 2007 with the Best Dissertation Award. He received his B.E. (1994) and M.S. (2001) both from Tsinghua University, China. At the University of Michigan-Shanghai Jiao Tong University Joint

Institute, his research work has been focused on robust/reliability based multidisciplinary design optimization and control, including topics such as multidisciplinary design optimization, robust/reliability control, sensitivity analysis, and system modeling.



Chengbin Ma (M'05) received the B.S.E.E. (Hons.) degree from East China University of Science and Technology, Shanghai, China, in 1997, and the M.S. and Ph.D. degrees both in the electrical engineering from University of Tokyo, Tokyo, Japan, in 2001 and 2004, respectively.

He is currently a tenure-track assistant professor of electrical and computer engineering with the University of Michigan-Shanghai Jiao Tong University Joint Institute, Shanghai Jiao Tong University, Shanghai, China. He is also with a joint faculty appointment in School of Mechanical Engineering, Shanghai Jiao Tong University. Between 2006 and 2008, he held a post-doctoral position with the Department of Mechanical and Aeronautical Engineering, University of California Davis, California, USA. From 2004 to 2006, he was a R&D researcher with Servo Laboratory, Fanuc Limited, Yamanashi, Japan. His research interests include networked hybrid energy systems, wireless power transfer, and mechatronic control.